

Effect of interacting dark energy on mass-temperature relation in galaxy clusters

Mahdi Naseri*

Department of Physics, K.N. Toosi University of Technology, P.O. Box 15875-4416, Tehran, Iran

Javad T. Firouzjaee[†]

*Department of Physics, K.N. Toosi University of Technology, P.O. Box 15875-4416, Tehran, Iran
and School of physics, Institute for Research in Fundamental Sciences (IPM),
P.O. Box 19395-5531, Tehran, Iran*



(Received 22 September 2020; accepted 11 November 2020; published 1 December 2020)

There is a variety of cosmological models for dark matter and dark energy in which a possible interaction is considered between these two significant components of the Universe. We focus on five suggested models of interacting dark matter and dark energy and derive the modified virial theorem for them by developing a previous approach. It provides an opportunity to study the evolution of this modified virial theorem with time and interacting constants for different interacting models. Then, we use this obtained virial condition to investigate the modified mass-temperature relation in galaxy clusters via three various methods. It reveals that the effect of interaction between dark matter and dark energy merely appears in the normalization factor of $M \propto T^{\frac{3}{2}}$. This relation also leads to a new constraint on the constants of interacting models, which only depends on the concentration parameter and density profile of the cluster. Then, we use five observational datasets to check some proposed figures for the constants of interaction which have resulted from other observational constraints. Finally, by fitting the observational results to the modified mass-temperature relation, we obtain values for interacting constants of three models and four specific cases of the two remaining models. In agreement with many other observational outcomes, we find that, according to observational data for masses and temperatures of the galaxy clusters, energy transfer occurs from dark matter to dark energy in the seven investigated models.

DOI: [10.1103/PhysRevD.102.123503](https://doi.org/10.1103/PhysRevD.102.123503)

I. INTRODUCTION

As different observational outcomes have revealed the existence of two unfamiliar contributors to the physics of the Universe, research into the “dark sector” has gained currency in modern cosmology. Dark matter (DM) was proposed to clarify rotation curves of spiral galaxies, and the idea behind dark energy (DE) was initially formed to explain the late-time acceleration of the Universe. Eventually, the Lambda cold dark matter (Λ CDM) model accounted for the primary suggestion for the cosmos.

In spite of gravitational evidence for DM from galaxies [1], clusters of galaxies [2], cosmic microwave background (CMB) anisotropies [3], cosmic shear [4], structure formation [5] and the large-scale structure of the Universe [6], last several years of direct and indirect searches of those DM particles did not give any convinced result [7]. In addition, the accelerated expansion of the Universe modeled with Λ [8] raised several problems, including the

“cosmological constant fine-tuning problem” and the “cosmic coincidence problem” [9].

However, it could be possible to assume and investigate more elaborate alternatives in which there is a feasible nongravitational interaction between DM and DE. The idea has extended in Ref. [10], where DM particle mass is determined according to its interaction with a scalar field with the energy density of DE. Such an assumption resembles how the Higgs field results in quark and lepton masses via interacting with them.

Not only is the notion of the interacting dark sector interesting, but it could also be beneficial in terms of solving some cosmological problems. By way of illustration, it may explain why the densities of DE and DM are of the same order, despite the fact that they evolve differently with redshift, namely the “coincidence problem” (see e.g., Ref. [11]). The interacting dark energy model should justify the same observation in contrast to the Λ CDM model, which modified gravity models do [12,13].

One can study the effects of modified gravity with structure formation and verified employing dark-matter-only N-body simulations [14]. Since experiments only

*mahdi.naseri@email.kntu.ac.ir
†firouzjaee@kntu.ac.ir

measure photons which are emitted from the baryonic matter, photons properties cannot be directly calculated only from dark matter simulations. However, hydrodynamical simulations are more appropriate in the observational aspect, as they provide observables, such as the halo profile, the turnaround radius [15], the splashback radius [16], and the mass-temperature (M-T) relation [17].

There is a wide range of observations, simulations, and theoretical research into the relationship between mass and temperature of galaxy clusters which have been done heretofore. The only consensus among all these endeavors is admission of an evident correlation between the total gravitational mass of the clusters, x-ray luminosity, and thereby their temperature (that is the temperature of the intracluster medium). It is of significance to study this relation, owing to the fact that the cluster masses are arduous to measure directly through observation. Fundamental arguments based on virialization density suggest that $M \propto T^{\frac{3}{2}}$, where T is the temperature of a cluster within a certain radius (e.g., the virial radius) and M is the mass within the same radius (see Refs. [18,19] for advanced discussion). The mass-temperature relation can be directly compared with observations. This relation has been used to put constraints on modified gravity models. For example, using the hydrodynamical simulations, Ref. [17] showed that the M-T relation obtained in modified gravity theories is different from the expectations of the general relativity. Nevertheless, Ref. [20] showed that the mass-temperature relation of the Λ CDM model is similar to that of the $f(R)$ and symmetron models.

The paper is organized as follows. Section II briefly presents the interacting dark energy model and specifically introduces five interacting models on which we concentrate in this study. We also obtain the virial theorem for these interacting models. Section III is devoted to the mass-temperature relation of galaxy clusters concerning the interaction between dark matter and dark energy. Section IV makes a comparison between observational data and the obtained M-T relation to study constants of interaction in the five models. We summarize and give our final thoughts in Sec. V.

II. INTERACTING DARK ENERGY MODELS AND VIRIAL THEOREM

The interacting dark energy model is composed of dark matter and dark energy only, as a flat Friedmann-Lemaître-Robertson-Walker (FLRW) background metric. The dark sector interaction is modeled with a heat flux in the Bianchi identities between the two dark components as

$$\nabla_{\mu} T_{(\lambda)}^{\mu\nu} \neq 0, \quad (1)$$

where $T_{(\lambda)}^{\mu\nu}$ in the energy-momentum tensor of each individual component, which is no longer conserved.

There are a number of interacting models which have been suggested and investigated recently. According to Ref. [11], the balance, Raychaudhuri, and FLRW equations can be written as

$$\dot{\rho}_b = -3H\rho_b, \quad (2)$$

$$\dot{\rho}_c = -3H\rho_c + Q, \quad (3)$$

$$\dot{\rho}_x = -3(1 + w_x)H\rho_x - Q, \quad (4)$$

$$\dot{H} = -4\pi G[\rho_b + \rho_c + (1 + w_x)\rho_x], \quad (5)$$

$$H^2 = \frac{8\pi G}{3}(\rho_b + \rho_c + \rho_x), \quad (6)$$

where H is the Hubble parameter, ρ_c is the cold dark matter density, ρ_b is the baryonic matter density, and ρ_x represents the density of dark energy [with $w_x < 0$ constant of its equation of state (EOS)].

Here, Q describes the rate of energy density transfer between DE and DM, which results from the interaction between them. For $Q > 0$, it describes the transfer of energy from DE to DM, and on the other hand, $Q < 0$ shows the transfer of energy from DM to DE. Note that baryons (b) and photons (γ) are not coupled to the dark sector; therefore, Q_{γ} and Q_b considered to be equal to zero.

A variety of functions has been proposed and studied for Q , including linear and nonlinear combinations of ρ_x and ρ_c . In this paper, we concentrate on five various models for Q , which are rather simple and common in the literature:

$$\text{model I: } Q = 3H(\alpha_c\rho_c + \alpha_x\rho_x),$$

$$\text{model II: } Q = 3H\xi_1 \frac{\rho_c\rho_x}{\rho_c + \rho_x},$$

$$\text{model III: } Q = 3H\xi_2 \frac{\rho_x^2}{\rho_c + \rho_x},$$

$$\text{model IV: } Q = 3H\xi_3 \frac{\rho_c^2}{\rho_c + \rho_x},$$

$$\text{model V: } Q = 3(\Gamma_c\rho_c + \Gamma_x\rho_x). \quad (7)$$

Here, ξ_1 , ξ_2 , ξ_3 , α_j , and Γ_j are the main parameters of interacting dark sector ($j = c, x$). The first four models are interesting, due to being coefficient with the Hubble parameter, which leads to more straightforward calculations, whereas model V is more complicated and has a physical meaning. According to this model, the oscillation inflaton field decays into relativistic particles during reheating process after inflation in the early Universe, and Γ_j describes decay width [11]. Constant parameters in models I to IV are dimensionless, while in model V, Γ_j has the dimension of the Hubble parameter. For further explanations about these choices for Q , look at Refs. [13,21].

A. Virial theorem in interacting models

In any theory of modified gravity, the virial theorem may significantly change from its Newtonian form. To find a virial relation in the context of general relativity, one has to use the covariant collisionless Boltzmann equation (see Ref. [22] and reference therein). This approach has been extended to the virial theorem in the modified gravity theories to study the dynamics of clusters of galaxies [23]. In homogeneous and isotropic background in which gravity is not strong, the virial theorem gets the Newtonian form.

Before analyzing mass-temperature relation in galaxy clusters, we have to investigate modifications to the virial theorem with regard to interacting dark sector. In order to achieve this objective, we derive the Layser-Irvine equation for models I to V and then use this equation to obtain the virial condition. This equation, and hence the virial theorem, has been driven in Ref. [24] for model I; however, we rewrite calculations so as to check it for the other four models, as well.

Considering model V, the perturbation equations for DE and DM in the subhorizon scale, which have been driven in Ref. [25], can be written in the real space as

$$\Delta'_c + \nabla_{\bar{r}} \cdot v_c = 3\Gamma_x(\Delta_x - \Delta_c)/R, \quad (8)$$

$$v'_c + \mathcal{H}v_c = -\nabla_{\bar{r}}\Psi - 3(\Gamma_c + \Gamma_x/R)v_c. \quad (9)$$

Here, \mathcal{H} indicates the Hubble parameter in the conformal time, v_c represents velocity of dark matter element, \bar{r} refers to conformal coordinates, and the prime denotes the derivative with respect to conformal time. Density contrasts of DM and DE are defined as $\Delta_c \approx \delta\rho_c/\rho_c = \delta_c$ and $\Delta_x \approx \delta\rho_x/\rho_x = \delta_x$, and we symbolize the dark energy to dark matter ratio by $R = \rho_c/\rho_x$. Moreover, $\Psi = \psi_m + \psi_d$ is the peculiar potential and is described by the Poisson equation,

$$\nabla^2\psi_j = 4\pi G(1 + 3w_j)\delta\rho_j, \quad (10)$$

where j stands for DM or DE. Considering $\nabla_r = \frac{1}{a}\nabla_{\bar{r}}$ and defining $\sigma_c = \delta\rho_c$ and $\sigma_x = \delta\rho_x$, Eqs. (8) and (9) can be written as

$$\dot{\sigma}_c + 3H\sigma_c + \nabla_r(\rho_c v_c) = 3(\Gamma_c\sigma_c + \Gamma_x\sigma_x), \quad (11)$$

$$\frac{\partial}{\partial t}(av_c) = -\nabla_r(a\psi_c + a\psi_x) - 3(\Gamma_c + \Gamma_x/R)(av_c), \quad (12)$$

where a is background scale factor and H is its Hubble parameter. Following the method of Refs. [24,26], we multiply both sides of Eq. (12) by $av_c\rho_c\hat{e}$ and then integrate them over the volume (\hat{e} indicates the volume element with criterion of expansion $\frac{\partial}{\partial t}\hat{e} = 3H\hat{e}$). For the left-hand side of Eq. (12), it is possible to write

$$\begin{aligned} \int av_c \frac{\partial}{\partial t}(av_c)\rho_c\hat{e} &= \int av_c(\dot{a}v_c + av'_c)\rho_c\hat{e} \\ &= \int a^2H\rho_c v_c^2\hat{e} + \int a^2\rho_c v_c v'_c \hat{e}. \end{aligned} \quad (13)$$

The kinetic energy K_c , which stems from the movement of DM particles, is defined as

$$K_c = \frac{1}{2} \int v_c^2 \rho_c \hat{e}. \quad (14)$$

It is possible to use this definition and write

$$\begin{aligned} \frac{\partial}{\partial t}(a^2K_c) &= 2a\dot{a}K_c + a^2 \frac{\partial}{\partial t}K_c \\ &= 2a^2HK_c + a^2 \left[\int v_c v'_c \rho_c \hat{e} + \frac{1}{2} \int v_c^2 \dot{\rho}_c \hat{e} \right. \\ &\quad \left. + \frac{1}{2} 3H \int v_c^2 \rho_c \hat{e} \right]. \end{aligned} \quad (15)$$

Using Eq. (15) in Eq. (13), we have

$$\begin{aligned} \int av_c \frac{\partial}{\partial t}(av_c)\rho_c\hat{e} &= \frac{\partial}{\partial t}(a^2K_c) - \frac{1}{2}a^2 \int v_c^2 \dot{\rho}_c \hat{e} \\ &\quad - \frac{1}{2}3Ha^2 \int v_c^2 \rho_c \hat{e}. \end{aligned} \quad (16)$$

Then, using Eq. (3) with Q of the model V in the last equation gives

$$\int av_c \frac{\partial}{\partial t}(av_c)\rho_c\hat{e} = \frac{\partial}{\partial t}(a^2K_c) - 3a^2(\Gamma_c + \Gamma_x/R)K_c. \quad (17)$$

For the first term in the right-hand side of Eq. (12), integration gives

$$\begin{aligned} & - \int av_c \nabla_r(a\psi_c + a\psi_x)\rho_c\hat{e} \\ &= a^2 \int \nabla_r(\rho_c v_c)\psi_c\hat{e} + a^2 \int \nabla_r(\rho_c v_c)\psi_x\hat{e}. \end{aligned} \quad (18)$$

With the aid of Eq. (11), it can be related to potential energy

$$\begin{aligned} & - \int av_c \nabla_r(a\psi_c + a\psi_x)\rho_c\hat{e} \\ &= -a^2(\dot{U}_{cc} + HU_{cc}) - a^2 \int \psi_x \frac{\partial}{\partial t}(\sigma_c\hat{e}) \\ &\quad + 3a^2\{\Gamma_c U_{cx} + \Gamma_x U_{xc} + 2\Gamma_c U_{cc} + 2\Gamma_x U_{xx}\}, \end{aligned} \quad (19)$$

where $U_{\alpha\beta} = \frac{1}{2} \int \sigma_\alpha \psi_\beta \hat{\epsilon}$; α and β stand for DM and DE, interchangeably.

Eventually, integrating the second term in the right-hand side of Eq. (12) leads to

$$- \int (av_c)^2 3(\Gamma_c + \Gamma_x/R) \rho_c \hat{\epsilon} = -6a^2(\Gamma_c + \Gamma_x/R) K_c. \quad (20)$$

Now, the Layzer-Irvine equation could be easily produced by combination of Eqs. (17), (19), and (20) as

$$\begin{aligned} \dot{K}_c + \dot{U}_{cc} + H(2K_c + U_{cc}) \\ = - \int \psi_x \frac{\partial}{\partial t} (\sigma_c \hat{\epsilon}) - 3(\Gamma_c + \Gamma_x/R) K_c \\ + 3\{\Gamma_c U_{cx} + \Gamma_x U_{xc} + 2\Gamma_c U_{cc} + 2\Gamma_2 U_{xx}\}. \end{aligned} \quad (21)$$

In virial equilibrium, the first and second terms of the previous equation are equal to zero. With the assumption of homogeneous distribution of DE, $\sigma_x = 0$, we get

$$K_c = - \frac{H - 6\Gamma_c}{2H + 3\Gamma_c + 3\Gamma_x/R} U_{cc}. \quad (22)$$

In order to facilitate following calculations, we define parameter λ_i and represent the virial condition as

$$K_c = -\lambda_i U_{cc}. \quad (23)$$

Obviously, λ_i is not necessarily equal to $\frac{1}{2}$ in interacting models and depends on interaction constants within \mathcal{Q} . The same procedure could be undergone for models I to IV. To sum up the results for all the five models, λ_i is ($i = I, II, III, IV, V$)

$$\begin{aligned} \text{model I: } \lambda_I &= \frac{1 - 6\alpha_c}{2 + 3\alpha_c + 3\alpha_x/R}, \\ \text{model II: } \lambda_{II} &= \frac{1 - \frac{6\xi_1}{R+1}}{2 + \frac{3\xi_1}{R+1}}, \\ \text{model III: } \lambda_{III} &= \frac{1}{2 + \frac{3\xi_2}{R(R+1)}}, \\ \text{model IV: } \lambda_{IV} &= \frac{1 - \frac{6R\xi_3}{R+1}}{2 + \frac{3R\xi_3}{R+1}}, \\ \text{model V: } \lambda_V &= \frac{H - 6\Gamma_c}{2H + 3\Gamma_c + 3\Gamma_x/R}. \end{aligned} \quad (24)$$

A constant of the EOS, w_j , has similar behavior for cold dark matter (CDM) and baryonic matter, that is $w_m = w_c = 0$. Thus, the Poisson equation or Eq. (10) leads to the same potential energy for both CDM and baryonic matter. It is very common to assume that baryons can

merely interact with dark sector via gravitational field. In this case, which we call "first possibility," Eq. (23) results in

$$K = K_c + K_b = -\lambda_i U_G. \quad (25)$$

Notwithstanding such a simple assumption, interaction between CDM and baryons might be considered a bit more intricate. Although both CDM and baryonic matter have the same potential function, they may interact separately, solely with their own type of matter. Given the circumstances, which we name "second possibility," Eq. (23) gives

$$K = - \left(\lambda_i \frac{\Omega_c}{\Omega_c + \Omega_b} + \frac{1}{2} \frac{\Omega_b}{\Omega_c + \Omega_b} \right) U_G, \quad (26)$$

where Ω is the relevant density parameter for each element of matter. In order to have brief calculations, we introduce parameter λ'_i and write the last equation as

$$\lambda'_i = \lambda_i \frac{\Omega_c}{\Omega_c + \Omega_b} + \frac{1}{2} \frac{\Omega_b}{\Omega_c + \Omega_b}, \quad (27)$$

$$K = -\lambda'_i U_G. \quad (28)$$

Equations (25) and (28) are the substitutes for the classical virial condition in dynamical equilibrium with respect to interaction between DE and DM (considering the first or the second possibility). It is apparent that these equations with $\alpha_j = \xi_1 = \xi_2 = \xi_3 = \Gamma_j = 0$ reduce to the familiar $K = -\frac{1}{2} U$ in noninteracting models.

Note that the assumption of homogeneous distribution of DE in Eq. (22) would be denied by nonstandard models of DE. As an example, detecting fewer clusters than the prediction of the primary CMB anisotropies via the Sunyaev-Zel'dovich effect by Planck satellite [27] has given rise to the idea of clustering DE. In this regime, DE contributes to clustering, and hence we cannot omit DE terms in Eq. (21), whereby the virial theorem changes to a more intricate form (see Refs. [28,29] to find out how clustering DE model alters characteristics of virialized haloes). In this work, we consider the common standard DE and postpone more investigations on the modified virial theorem with respect to DE with negligible sound speeds to future studies.

III. MASS TEMPERATURE RELATION OF GALAXY CLUSTERS

The primary approach to form mass-temperature relation is combining the virial theorem with conservation of energy, which brings about $M \propto T^\zeta$. While the power-law index appears to be $\zeta = \frac{3}{2}$ in most masses, a "break" is predicted in a myriad of observations and simulations at low masses, which gives rise to $\zeta > \frac{3}{2}$ in this particular

range. The physics behind this behavior has been under study for a while; Ref. [30] attributed it to the cooling process, and the heating process is stated in Ref. [31] to be the rationale for this break, to name but a few. In order to reconstruct theories concerning this break, Afshordi and Cen have attributed it to the nonsphericity of the initial protoclusters in Ref. [18], and Popolo has taken the angular momentum acquisition by protoclusters into account in Ref. [19]. Nevertheless, more recent studies, embracing Refs. [32,33], revealed that there is no evidence of a double slope in the M-T relation. However, the existence of this break is still under discussion.

We try to take a look at three different methods which have been provided by Afshordi and Cen and Popolo to reconstruct the mass-temperature relation in galaxy clusters, considering the modified virial theorem for interacting dark matter and dark energy. The double slope in the mass-temperature relation is not our principal focus, and we neglect it, although there will be some mentions of that.

A. Derivation of mass-temperature relation

In this section, we develop the method used by Afshordi and Cen in Ref. [18] to rebuild the M-T relation in galaxy clusters for interacting models. They begin with a definition of the kinetic and potential energies and pursue calculations by using velocity as a function of the gravitational potential in the perturbation theory, Poisson equation, and Gauss's theorem to obtain the initial energy of a protocluster (i.e., E_{ta} or the total energy of that at turnaround radius r_{ta}). Since up to this point there is no indication of interacting dark sector, we avoid repeating calculations, and we just mention the outcome obtained in Ref. [18]:

$$E_{\text{ta}} = -\frac{10\pi G}{3}\rho_{\text{ta}}^2 r_{\text{ta}}^5 B. \quad (29)$$

Here, B is defined as

$$B \equiv \int_0^1 \tilde{\delta}_{\text{ta}}(\tilde{r})(1 - \tilde{r}^2)d^3\tilde{r}, \quad (30)$$

where $\tilde{r} \equiv \frac{r}{r_{\text{ta}}}$, $\tilde{\delta}_{\text{ta}} \equiv \delta_{\text{ta}} + \frac{3}{5}(\Omega_{\text{ta}} - 1)$ and Ω_{ta} and δ_{ta} are density parameter and density contrast at turnaround time, respectively.

Taking a surface pressure term into account (which is exerted at the boundary of the cluster), the virial condition gives

$$K_{\text{vir}} + E_{\text{vir}} = (1 - 2\lambda_i)U_{\text{vir}} + 3P_{\text{ext}}V. \quad (31)$$

There is the point where the impact of interacting dark sector emerges. Here, P_{ext} denotes the pressure on the outer boundary of the virialized cluster, and V stands for the volume. It is clear that the last equation could reduce to the

classical equation (used by Afshordi and Cen), if $\lambda_i = \frac{1}{2}$. Another equation for surface pressure is expressed by

$$3P_{\text{ext}}V = -\nu U_{\text{vir}}, \quad (32)$$

where the parameter ν is a coefficient constant to indicate the considered correlation between exerted pressure and the potential energy. Combining the two preceding equations gives

$$K_{\text{vir}} + E_{\text{vir}} = (1 - 2\lambda_i - \nu)U_{\text{vir}}. \quad (33)$$

The surface pressure term also alters the relation between kinetic and potential energy after virialization to

$$K_{\text{vir}} = -\frac{2\lambda_i + \nu}{2}U_{\text{vir}}. \quad (34)$$

Inserting U_{vir} from Eq. (34) into Eq. (33) leads to

$$-\frac{2\lambda_i + \nu}{2 - 2\lambda_i - \nu}E_{\text{vir}} = K_{\text{vir}}. \quad (35)$$

Then, the kinetic energy of the cluster can be separated into fully ionized baryonic gas and DM as

$$K_{\text{vir}} = \frac{3}{2}M_c\sigma_v^2 + \frac{3M_b k_B T}{2\mu m_p}, \quad (36)$$

where σ_v stands for the mass-weighted mean velocity dispersion of DM particles in one dimension, M_b is the total baryonic mass, k_B is the Boltzmann constant, T is the temperature, $\mu = 0.59$ is the mean molecular weight, and m_p represents the proton mass. To simplify the previous equation, $\tilde{\beta}_{\text{spec}}$ is defined as

$$\tilde{\beta}_{\text{spec}} = \beta_{\text{spec}} \left[1 + (f\beta_{\text{spec}}^{-1} - 1) \frac{\Omega_b}{\Omega_b + \Omega_c} \right]. \quad (37)$$

Here, f is the fraction of baryonic matter in hot gas, and $\beta_{\text{spec}} \equiv \sigma_v^2 / (k_B T / \mu m_p)$. This definition assists to obtain from Eq. (36)

$$K_{\text{vir}} = \frac{3\tilde{\beta}_{\text{spec}} M k_B T}{2\mu m_p}. \quad (38)$$

Now, using Eqs. (29) and (38) in Eq. (35), with respect to conservation of energy ($E_{\text{ta}} = E_{\text{vir}}$), we find

$$k_B T = \frac{5\mu m_p}{8\pi\tilde{\beta}_{\text{spec}}} \left(\frac{2\lambda_i + \nu}{2 - 2\lambda_i - \nu} \right) H_{\text{ta}}^2 r_{\text{ta}}^2 B. \quad (39)$$

In order to find an expression for $H_{\text{ta}}^2 r_{\text{ta}}^2$, parameter e is defined to be the energy of a test particle with unit mass at r_{ta} ; therefore, we can write it as

$$e = \frac{v_{\text{ta}}^2}{2} - \frac{GM}{r_{\text{ta}}}. \quad (40)$$

We also have collapse time (or dynamical timescale) as

$$t = \frac{2\pi GM}{(-2e)^{3/2}}. \quad (41)$$

With the assumption that this time is approximately equal to the required time for virialization, and using the Friedmann equations, one can obtain

$$-2e = \frac{5}{4\pi} H_{\text{ta}}^2 r_{\text{ta}}^2 A = \left(\frac{2\pi GM}{t} \right)^{2/3}, \quad (42)$$

$$A \equiv \int_0^1 \tilde{\delta}_i(\tilde{r}) d^3\tilde{r} = \frac{2}{5} \left(\frac{3\pi^4}{t^2 G \rho_{\text{ta}}} \right)^{1/3}. \quad (43)$$

Using the last two equations together with Eq. (39), the mass-temperature relation can be obtained:

$$k_B T = \left(\frac{\mu m_p}{2\tilde{\beta}_{\text{spec}}} \right) \left(\frac{2\lambda_i + \nu}{2 - 2\lambda_i - \nu} \right) \left(\frac{2\pi GM}{t} \right)^{2/3} \left(\frac{B}{A} \right). \quad (44)$$

By inserting numerical values, this relation can be written as

$$k_B T = (6.62 \text{ keV}) \tilde{Q} \left(\frac{M}{10^{15} h^{-1} M_{\odot}} \right)^{2/3}, \quad (45)$$

where the dimensionless factor \tilde{Q} is defined:

$$\tilde{Q} \equiv \left(\frac{\tilde{\beta}_{\text{spec}}}{0.9} \right)^{-1} \left(\frac{2\lambda_i + \nu}{2 - 2\lambda_i - \nu} \right) \left(\frac{B}{A} \right) (Ht)^{-2/3}. \quad (46)$$

Equation (45) is the mass-temperature relation in galaxy clusters, regarding interaction between DE and DM. It is noticeable that the effect of the interacting dark sector merely appears in factor \tilde{Q} . Afshordi and Cen extensively discuss this factor in Ref. [18]. Overall, $\tilde{\beta}_{\text{spec}}$ is a function of the ratio of the kinetic energy per unit mass of DM to the thermal energy of gas particles (β_{spec}), the fraction of baryonic matter in hot gas (f), and the ratio of baryonic matter to DM in the sphere. According to different simulations and observations, these three parameters vary slightly, whereby the final value for $\tilde{\beta}_{\text{spec}}$ does not face dramatic changes and is close to 0.9; hence, we fix it by this figure in our calculations. The second variable, ν , depends on density profile $f(\omega)$ and concentration parameter c , which is given by

$$\nu(c, f(\omega)) \equiv -\frac{3P_{\text{ext}} V}{U} = \frac{c^3 \int_c^\infty f(\omega) g(\omega) \omega^{-2} d\omega}{\int_0^c f(\omega) g(\omega) \omega d\omega}, \quad (47)$$

where

$$g(\omega) = \int_0^\omega f(\omega) \omega^2 d\omega. \quad (48)$$

For the density profile, we may choose the Navarro-Frenk-White (NFW) profile as:

$$f_{\text{NFW}}(\omega) = \frac{1}{(\omega)(1+\omega)^2}, \quad (49)$$

where $\omega = \frac{r}{r_s}$ and r_s is the scale radius given in [34]. This profile is proposed by Navarro, Frenk, and White and has been widely used and studied in the literature. However, there have been some objections to that, as some recent observations have revealed a cored density profile in the inner region of the haloes. Several density profiles have been proposed to include the cored central region, including the Burkert profile [35], which is expressed by

$$f_{\text{Burkert}}(\omega) = \frac{1}{(1+\omega)(1+\omega^2)}. \quad (50)$$

Clearly, considering each of these profiles may affect the M-T relation, as well as the other properties of clusters.

Concentration parameter c is defined as the ratio of virial radius to scale radius, that is $\frac{r_{\text{vir}}}{r_s}$. The density profile is exclusively described by c . In case there are not any observational data, the following relation (from Ref. [36]) may be used to find the value of the concentration parameter,

$$c = 8.3 \left(\frac{M_{200}}{10^{12} M_{\odot}} \right)^{-0.104}, \quad (51)$$

where M_{200} is the mass enclosed by the radius in which the average density is 200 times the critical density of the Universe. Meanwhile, the mass-concentration relation has extensively been under study, and it would have minuscule differences in various works, such as Ref. [37].

In Eq. (46), parameter $\left(\frac{B}{A} \right)$ plays the prominent role in the break of mass-temperature relation in low masses. In spite of the fact that both A and B are proportional to scale factor, $\frac{A}{B}$ remains constant. Considering an initial density profile with multiple peaks (rather than a homogeneous distribution of density, or a profile with one central peak), Afshordi and Cen obtain

$$\left\langle \frac{B}{A} \right\rangle = \frac{4(1-n)}{(n-5)(n-2)} \left[1 - \frac{n(n+3)}{10(1-n)} (1 - \Omega_c - \Omega_b - \Omega_\Lambda) \right] \times \left(\frac{Ht}{\pi(\Omega_c + \Omega_b)} \right)^{2/3}, \quad (52)$$

where n is the index of the density power spectrum. Choosing an initial density profile with multiple peaks would be more comprehensive and rational because, in hierarchical structure formation models, mass gradually accumulates in several regions of the initial cluster and not solely around the center. Taking nonsphericity in the geometry of the collapsing protocluster into account, which has a notable sign in low masses, Afshordi and Cen write some equations for dispersion of factor $\frac{A}{B}$, or $\frac{\Delta B}{A}$. It reveals more dispersion in low masses and consequently leads to a so-called break in the M-T relation. However, as we have mentioned before, not only is there no agreement on the existence of this double slope, but there is also no sign of interacting dark sector in this parameter; thus, we neglect it for our study.

Furthermore, another parameter is introduced in Ref. [18] as

$$y = \frac{B}{A(Ht)^{\frac{2}{3}}}. \quad (53)$$

This definition changes Eq. (46) to a more straightforward form. It can be written as a function of density profile and concentration parameter,

$$y(c, f) = \frac{\Delta^{1/3}(2 - 2\lambda_i - \nu)c \int_0^c f(\omega)g(\omega)\omega d\omega}{3\pi^{2/3}g^2(c)}, \quad (54)$$

where Δ is the overdensity of the sphere and for a virialized cluster is somewhere in the region of $\Delta = 200$, meaning that the cluster has an average density of 200 times as much as critical density of the Universe. The last relation is driven in Ref. [18] regarding the virial theorem and the definition of ν ; meanwhile, owing to modification of the virial theorem, the factor $(1 - \nu)$ has changed to $(2 - 2\lambda_i - \nu)$ for interacting models.

Both the mass and temperature of a cluster have to be positive to result in a genuine outcome. Combining this principle with Eq. (46) shows a constraint on the possible values for λ_i . As all contributors in Eq. (46) are positive quantities, the ratio $(\frac{2\lambda_i + \nu}{2 - 2\lambda_i - \nu})$ should be positive. As a result, we should have either

$$-\frac{\nu}{2} < \lambda_i < \frac{2 - \nu}{2}, \quad (55)$$

or

$$\frac{2 - \nu}{2} < \lambda_i < -\frac{\nu}{2}. \quad (56)$$

Due to the fact that ν is always a positive parameter, Eq. (56) necessitates a negative λ_i . Taking Eq. (25) into account, a negative λ_i does not have any physical meaning;

thus, just Eq. (55) could be acceptable as a criterion for the value of λ_i , and its more accurate form is

$$0 < \lambda_i < \frac{2 - \nu}{2}. \quad (57)$$

Note that Eq. (46) is derived for our first possibility. It is self-evident that by replacing λ_i with λ'_i we would also be able to study the second possibility.

B. Reforming the top-hat model

In order to form the break in the M-T relation, Del Popolo takes angular momentum acquisition of the collapsing protoclusters into consideration in Ref. [19] and later reinforces this method by adding another term for dynamical friction in Ref. [20]. The angular momentum is acquired by interacting with neighboring protoclusters. Del Popolo suggests two approaches to formulate the M-T relation. The first approach is based upon the development of the top-hat model, and we investigate it in this section, with an additional assumption of the interacting dark sector.

To start this method, an ensemble of gravitationally growing mass concentrations is assumed, and then with the assistance of the Liouville's theorem, Del Popolo obtains the radial acceleration of a particle as

$$\frac{dv_r}{dt} = -\frac{GM}{r^2} + \frac{L^2(r)}{M^2 r^3} + \frac{\Lambda}{3}r - \eta \frac{dr}{dt}, \quad (58)$$

where η is the dynamical friction coefficient and $L(r)$ denotes the acquired angular momentum in radius r from the center of the cluster. $L(r)$ has a very complicated relation, which can be found in Refs. [38,39]. Integrating the previous equation leads to

$$\frac{1}{2} \left(\frac{dr}{dt} \right)^2 = \frac{GM}{r} + \int_0^r \frac{L^2}{M^2 r^3} dr + \frac{\Lambda}{6}r^2 - \int_0^r \eta \frac{dr}{dt} + \epsilon, \quad (59)$$

Here, ϵ is the specific binding energy of the shell and can be determined by condition of $\frac{dr}{dt} = 0$ at r_{ta} . The preceding equation represents four forms of potential energy; using them in the modified virial condition for interacting dark sector, we have

$$\langle K \rangle = -\lambda_i \langle U_G \rangle - \langle U_L \rangle + \langle U_\Lambda \rangle + \langle U_\eta \rangle. \quad (60)$$

Here, $\langle \rangle$ indicates time averaged value of any quantity. By using Eq. (32) and (33) in the previous equation, we get

$$\langle K \rangle = (2\lambda_i + \nu) \left(-\frac{1}{2} \langle U_G \rangle - \langle U_L \rangle + \langle U_\Lambda \rangle + \langle U_\eta \rangle \right). \quad (61)$$

Defining r_{eff} as the time averaged radius of mass shell, Eq. (61) can be written as

$$\begin{aligned} \langle K \rangle &= -\left(\frac{2\lambda_i + \nu}{2}\right) U_G \left[1 + 2\frac{U_L}{U_G} - 2\frac{U_\Lambda}{U_G} - 2\frac{U_\eta}{U_G} \right] \\ &= \left(\frac{2\lambda_i + \nu}{2}\right) \frac{GM}{r_{\text{eff}}} \left[1 + 2\frac{r_{\text{eff}}}{GM^3} \int_0^{r_{\text{eff}}} \frac{L^2(r)}{r^3} dr - \frac{\Lambda r_{\text{eff}}^3}{3GM} - 2\frac{r_{\text{eff}}}{GM} \int_0^{r_{\text{eff}}} \eta \frac{dr}{dt} \right]. \end{aligned} \quad (62)$$

The ratio of r_{eff} to r_{ta} is defined by $\psi = \frac{r_{\text{eff}}}{r_{\text{ta}}}$; then, we have

$$M = 4\pi\rho_b x_1^3/3, \quad \chi = r_{\text{ta}}/x_1, \quad \Omega_0 = \frac{8\pi G\rho_b}{3H_0^2}, \quad (63)$$

and as a result,

$$r_{\text{eff}} = \psi\chi \left(\frac{2GM}{\Omega_0 H_0^2} \right)^{1/3}. \quad (64)$$

Then, putting $\langle K \rangle$ from Eq. (38) into Eq. (62) results in the M-T relation as

$$\begin{aligned} \frac{k_B T}{\text{keV}} &= 1.58(\lambda_i + \nu) \frac{\mu}{\beta_{\text{spec}} \psi \chi} \Omega_0^{1/3} \left(\frac{M}{10^{15} M_\odot h^{-1}} \right)^{2/3} (1 + z_{\text{ta}}) \times \left[1 + \left(\frac{32\pi}{3} \right)^{2/3} \psi \chi \rho_{b,\text{ta}}^{2/3} \frac{1}{H_0^2 \Omega_{b,0} M^{8/3} (1 + z_{\text{ta}})} \right. \\ &\quad \left. \times \int_0^{r_{\text{eff}}} \frac{L^2}{r^3} dr - \frac{2}{3} \frac{\Lambda}{\Omega_{b,0} H_0^2 (1 + z_{\text{ta}})^3} (\psi \chi)^3 - \frac{2^{10/3}}{3^{2/3}} \pi^{2/3} \left(\frac{\psi \chi}{\Omega_{b,0} H_0^2} \right) \left(\frac{\rho_{b,0}}{M} \right)^{2/3} \frac{1}{1 + z_{\text{ta}}} \times \int \eta \frac{dr}{dt} dr \right]. \end{aligned} \quad (65)$$

Conservation of energy should be used in order to determine the value of ψ , or r_{eff} , as

$$\langle E \rangle = \langle K \rangle + \langle U_G \rangle + \langle U_\Lambda \rangle + \langle U_L \rangle + \langle U_\eta \rangle = U_{G,\text{ta}} + U_{\Lambda,\text{ta}} + U_{L,\text{ta}} + U_{\eta,\text{ta}}. \quad (66)$$

Using Eq. (61) in this equation, we find

$$\frac{-2\lambda_i - \nu + 2}{2} \langle U_G \rangle - (2\lambda_i + \nu - 1) \langle U_L \rangle + (2\lambda_i + \nu + 1) (\langle U_\Lambda \rangle + \langle U_\eta \rangle) = U_{G,\text{ta}} + U_{\Lambda,\text{ta}} + U_{L,\text{ta}} + U_{\eta,\text{ta}}, \quad (67)$$

and with the aid of the method provided by Ref. [40] for the last equation, the cubic equation is obtained,

$$\begin{aligned} (-2\lambda_i - \nu + 2) + (\chi\psi)^3 (2\lambda_i + \nu + 1) \Upsilon - \psi(2 + \Upsilon\chi^3) - \frac{27}{32} \frac{\chi^9 \psi}{\rho_{\text{ta}}^3 \pi^3 G r_{\text{ta}}^8} \left[(2\lambda_i + \nu - 1) \int_0^{r_{\text{eff}}} \frac{L^2(r)}{r^3} dr + \int_0^{r_{\text{ta}}} \frac{L^2(r)}{r^3} dr \right. \\ \left. - \frac{16\pi^2}{9} (2\lambda_i + \nu + 1) \rho_{\text{ta}}^2 r_{\text{ta}}^6 \times \left(\int_0^{r_{\text{eff}}} \eta \frac{dr}{dt} dr - \frac{1}{2\lambda_i + \nu + 1} \int_0^{r_{\text{ta}}} \eta \frac{dr}{dt} dr \right) \right] = 0, \end{aligned}$$

with

$$\Upsilon = \frac{\Lambda}{4\pi G \rho_{\text{ta}}} = \frac{\Lambda r_{\text{ta}}^3}{3GM} = \frac{2\Omega_\Lambda}{\Omega_0} \left(\frac{\rho_{\text{ta}}}{\rho_{\text{ta},b}} \right)^{-1} (1 + z_{\text{ta}})^{-3}. \quad (68)$$

Then, it is possible to find ψ , or r_{eff} , by solving the above equation. Note that the M-T relation or Eq. (65) can be expressed in terms of r_{vir} as

$$\begin{aligned} \frac{k_B T}{\text{keV}} &= 0.94(2\lambda_i + \nu) \frac{\mu}{\beta_{\text{spec}}} \left(\frac{r_{\text{ta}}}{r_{\text{vir}}} \right) \left(\frac{\rho_{\text{ta}}}{\rho_{b,\text{ta}}} \right)^{1/3} \Omega_0^{1/3} \left(\frac{M}{10^{15} M_\odot h^{-1}} \right)^{2/3} (1 + z_{\text{ta}}) \left[1 + \frac{15 r_{\text{vir}} \rho_{b,\text{ta}}}{\pi^2 H_0^2 \Omega_0 \rho_{\text{ta}}^3 r_{\text{ta}}^9 (1 + z_{\text{ta}})} \int_0^{r_{\text{vir}}} \frac{L^2(r) dr}{r^3} \right. \\ &\quad \left. - \frac{2}{3} \frac{\Lambda}{H_0^2 \Omega_0} \left(\frac{r_{\text{vir}}}{r_{\text{ta}}} \right)^3 \left(\frac{\rho_{b,\text{ta}}}{\rho_{\text{ta}}} \right) \frac{1}{(1 + z_{\text{ta}})^3} - \frac{6^{1/3}}{\pi^{1/3}} r_{\text{vir}} r_{\text{ta}} \left(\frac{\rho_{b,\text{ta}}}{\rho_{\text{ta}}} \right)^{1/3} \left(\frac{\rho_{b,0}}{M} \right)^{2/3} \frac{1}{1 + z_{\text{ta}}} \times \frac{\lambda_0}{1 - \mu(\delta)} \right], \end{aligned} \quad (69)$$

where $\mu(\delta)$ and λ_0 are parameters related to dynamical friction and are given in Ref. [41].

The previous equation has been obtained for the mass-temperature relation of galaxy clusters, considering the effects of angular momentum acquisition (in Ref. [19]), dynamical friction (in Ref. [20]), and eventually the impact of interacting dark sector (in this paper). As can be seen, λ_i plays a more profound role in this approach, in comparison with Afshordi and Cen's method, owing to its contribution to both Eqs. (68) and (69). Similar to the preceding model, λ'_i could be substituted for λ_i to create the second possibility in all equations.

This model is based on the assumption of cluster formation with the evolution of a spherical top-hat density perturbation, and the "late-formation approximation." The latter approximation states that any cluster at redshift z is has just reached its virialization. Although it is a good assumption in some cases, including the critical case of $\Omega_0 = 1$ (where the cluster formation is rapid), it constructs impediments to other cosmological models.

C. Continuous formation model

After a discussion on limitations and disadvantages to the former model in Ref. [19], Del Popolo derives the M-T relation concerning the continuous formation model, which had been used in Ref. [42] before. In this model, cluster formation occurs gradually, instead of instantaneously. The effects of angular momentum and dynamical friction with respect to this approach have been studied in Refs. [19,20], respectively. Now, we are going to study how interacting dark sector makes a difference in the M-T relation in terms of this procedure.

By integrating Eq. (58), Del Popolo obtains an expression for the ratio of the total energy of a virialized cluster to its mass or $\frac{E}{M}$. We avoid iterating calculations, so the result is

$$\frac{E}{M} = \frac{3m}{10(m-1)} \left(\frac{2\pi G}{t_\Omega} \right)^{\frac{2}{3}} M^{\frac{2}{3}} \left[\frac{1}{m} + \left(\frac{t_\Omega}{t} \right)^{2/3} + \frac{K(m, x)}{(M/M_0)^{8/3}} + \frac{\lambda_0}{1 - \mu(\delta)} + \frac{\Lambda \chi^3}{3H_0^2 \Omega_{b,0}} \right], \quad (70)$$

where

$$\begin{aligned} t_\Omega &= \frac{\pi \Omega_0}{H_0 (1 - \Omega_0 - \Omega_\Lambda)^{\frac{3}{2}}}, \\ K(m, x) &= (m-1) Fx \text{LerchPhi}(x, 1, 3m/5 + 1) \\ &\quad - (m-1) F \text{LerchPhi}(x, 1, 3m/5), \\ \text{LerchPhi}(x', y', z') &= \sum_{n=0}^{\infty} \frac{x'^n}{(z' + n)^{y'}}, \\ F &= \frac{2^{7/3} \pi^{2/3} \chi \rho_b^{2/3}}{3^{2/3} H^2 \Omega} \int_0^r \frac{L^2(r) dr}{r^3}, \\ x &= 1 + \left(\frac{t_\Omega}{t} \right)^{2/3}. \end{aligned} \quad (71)$$

Meanwhile, $M = M_0 x^{-3m/5}$, and M_0 is given in Ref. [42].

Combining Eqs. (70) and (38) with the virial theorem results in

$$k_B T = \frac{4}{3} \tilde{a} \frac{\mu m_p}{2\beta_{\text{spec}}} \frac{E}{M}, \quad (72)$$

and afterwards

$$\begin{aligned} \frac{k_B T}{\text{keV}} &= \frac{2}{5} \tilde{a} \frac{\mu m_p}{2\beta_{\text{spec}}} \frac{m}{m-1} \left(\frac{2\pi G}{t_\Omega} \right)^{2/3} M^{2/3} \\ &\times \left[\frac{1}{m} + \left(\frac{t_\Omega}{t} \right)^{2/3} + \frac{K(m, x)}{(M/M_0)^{8/3}} + \frac{\lambda_0}{1 - \mu(\delta)} + \frac{\Lambda \chi^3}{3H_0^2 \Omega_{b,0}} \right]. \end{aligned} \quad (73)$$

Here, the parameter \tilde{a} is the ratio of the kinetic to total energy of the cluster, and according to Eq. (35), we have

$$\tilde{a} = \frac{2\lambda_i + \nu}{2 - 2\lambda_i - \nu}. \quad (74)$$

Thus, we can see that the trace of interacting dark sector emerges in a factor in the M-T relation. Like in the previous procedures, putting λ'_i instead of λ_i gives the equation for the second possibility.

IV. RESULTS AND DISCUSSION

We use five different sets of observational data to determine constants of the interacting dark sector for models I to V, with the aid of the M-T relation [Eq. (45)]. These observational datasets are provided in Refs. [43–47]. The first set provides details of mass and temperature for 32 clusters (hereafter "Obs. 1999"). The second source of data is used by Afshordi and Cen in Ref. [18] and consists of 39 clusters (hereafter "Obs. 2001"). The third dataset includes Chandra's observations for ten low-redshift clusters (hereafter "Obs. 2006"), and details of 49 low-redshift clusters from Chandra are collected in the fourth dataset (hereafter "Obs. 2009"). Finally, the last resource comprises 20 clusters from XMM-Newton observations (hereafter "Obs. 2015").

Measurements of temperature are generally based on x-ray observations; hence, the temperatures given in the mentioned catalogs are x-ray temperature and could be different than density-weighted temperature in Eq. (45), which is averaged over the whole cluster. The reason lies within the fact that x-ray temperature (T_X) is exclusively measured over the central brighter portion of the cluster. To convert x-ray temperature to T in Eq. (45), we use the relation below from Ref. [48]:

$$T = T_X [1 + (0.22 \pm 0.05) \log_{10} T_X (\text{keV}) - (0.11 \pm 0.03)]. \quad (75)$$

As has been mentioned before, it is prevalent to consider the overdensity of the virialized clusters to be about 200 times the critical density of the Universe. Therefore, M_{200} is considered to be the cluster mass after virialization. The masses given in Obs. 1999 to 2015 have been obtained with respect to different methods, and none of them incorporates M_{200} . In order to convert these masses to M_{200} (e.g., M_{500} to M_{200}), we use the relation $M_\delta \propto \delta^{-0.266}$ from Ref. [49], where $\delta = \frac{M(<r)}{\frac{4}{3}\pi\rho_c r^3}$. This relation has been obtained via fitting the relation of $M \propto T^{\frac{3}{2}}$ to simulation data, regarding different values of δ . As our calculations revealed, considering interaction between DM and DE has no impact on density profile, and it only affects the factor of the M-T relation. Therefore, this relation can be used for mass conversion.

Our aim is to fit observational data between M_{200} and T to the relation of $M \propto T^{\frac{3}{2}}$, in order to find the matched value of λ_i in the coefficient factor for each fit and each model and then determine the interacting constants. In addition, some values for constants of the interacting dark sector have been recently proposed in Ref. [13] for models II, III, IV, and two special cases of model I, based on various observations. Observations related to Type-Ia Supernovae (SNe Ia), the present value of the Hubble parameter (H_0), cosmic chronometers (CC), baryon acoustic oscillations (BAOs), and the Planck measurements of the CMB temperature anisotropy (Planck TT) are the five types of observation which make up constraints in Ref. [13] to find constants of the interacting dark sector. We also use those proposed values in the M-T relation to make comparison among outcomes and observational datasets for mass and temperature.

Model I is expressed by two interacting constants, namely α_x and α_c . Two specific and simple cases for this model are $\alpha_x = 0$ and $\alpha_c = 0$. Figure 1 compares the mass-temperature relation under the assumption of $\alpha_x = 0$ for model I with observational datasets, based on the values obtained in Ref. [13]. According to Ref. [13], observations of “ $SNeIa + H_0$ ” and “ $SNeIa + H_0 + CC$ ” result in $\alpha_c = -0.36$ and $\alpha_c = -0.092$, respectively. These two values are not consistent with the constraint of Eq. (57) and give the unreal negative temperatures for given masses. The outcome of $\alpha_c = -0.0019$, which is obtained from “ $SNeIa + H_0 + CC + BAO$,” is illustrated with red lines in Fig. 1. Likewise, the constraint of “ $PlanckTT$ ” has given $\alpha_c = -9.73 \times 10^{-5}$, and its result in the M-T relation is shown with black lines. For both predictions, solid lines are related to the first possibility of the NFW density profile, while dotted lines are attributed to the second possibility for the same density profile. The results of the Burkert density profile are presented by dashed lines (for the first possibility) and dot-dashes lines (for the second possibility). Note that the differences between first and second possibilities are very subtle in this model, whereby solid and dotted black lines are almost indistinguishable. Datasets and their

fitted curves for Obs. 1999, 2001, 2006, 2009, and 2015 are demonstrated with colors cyan, magenta, blue, green, and brown, respectively (the fitted lines for Obs. 1999 and 2001 are virtually coincident).

We immediately infer that for the case of $\alpha_x = 0$ in model I a negative α_c has to be very close to zero to not violate the constraint of Eq. (57). However, these values are not consistent with any observational dataset.

Figure 2 indicates the M-T relation for another special case for model I, which is $\alpha_c = 0$. Chosen colors and types of lines are the same as Fig. 1, and, again, results of $SNeIa + H_0$ (with $\alpha_x = -0.26$) and $SNeIa + H_0 + CC$ (with $\alpha_c = -0.27$) violate the constraint of Eq. (57) and consequently cannot be presented, whereas observations of $SNeIa + H_0 + CC + BAO$ (with $\alpha_x = -0.037$) and $PlanckTT$ (with $\alpha_x = -0.0052$) are theoretically acceptable. Here, the difference between the first and second possibilities is easier to spot, in comparison with the former case. As can be seen, these predicted values lead to higher masses than observational data, like in the previous case.

The value of λ_i explains the ratio of kinetic to potential energy after virialization and plays the most vital role in our calculations. Figure 3 reveals how λ and λ' change as a function of α_c or α_x , in two mentioned cases of model I, which are more simple. The blue lines are related to model I with $\alpha_x = 0$, and the red lines describe the same model with $\alpha_c = 0$. Therefore, the horizontal axis is attributed to α_c in

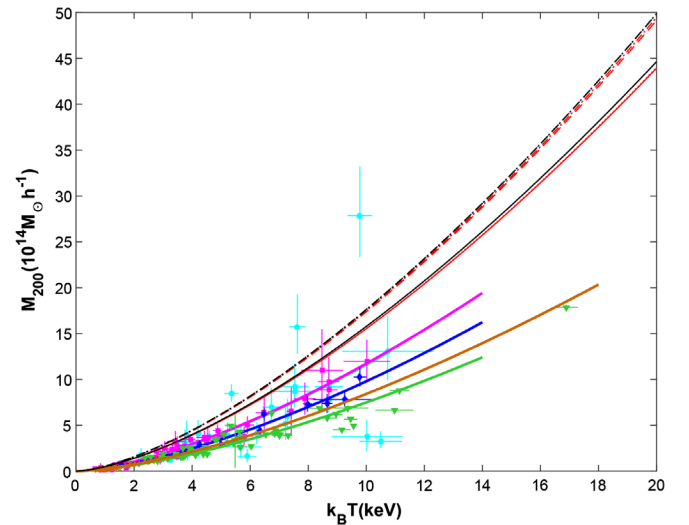


FIG. 1. The behavior of the mass-temperature relation in interacting model I, in special case of $\alpha_x = 0$. Red lines indicate the outcome of $SNeIa + H_0 + CC + BAO$ observations for α_c , and black lines display the prediction related to $PlanckTT$ observations for this parameter. The other five colors denote five observational datasets from 1999 to 2015 (Obs. 1999: cyan; Obs. 2001: magenta; Obs. 2006: blue; Obs. 2009: green; Obs. 2015: brown). Solid and dotted lines show the first and second possibilities for NFW density profile, while dashed and dot-dashed lines illustrate these two possibilities for the Burkert profile, respectively.

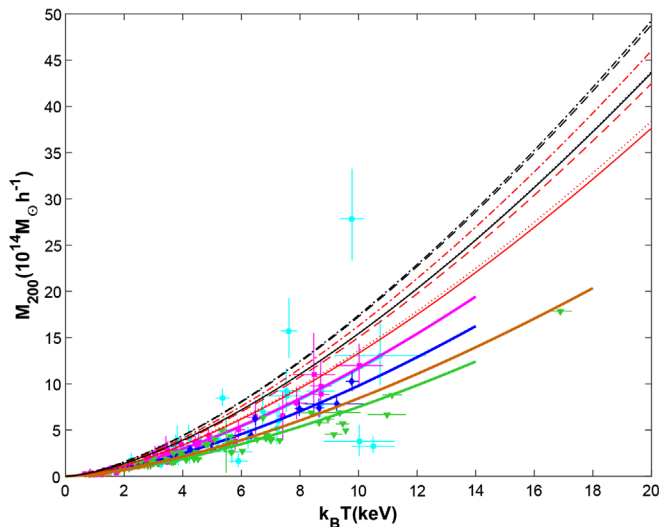


FIG. 2. Comparison between observational data and the predictions of $SNeIa + H_0 + CC + BAO$ and $PlanckTT$ observations for the case of $\alpha_c = 0$ in model I. Colors and types of lines are chosen the same as in Fig. 1.

the former case and to α_x in the latter one. Moreover, solid lines are shown as the symbol of the first possibility, and the dotted lines denote the second possibility. The black dashed line is drawn with respect to the obtained value of λ_I for Obs. 1999 (first possibility), and the dot-dashed line shows the same value, but regarding the second possibility. We do

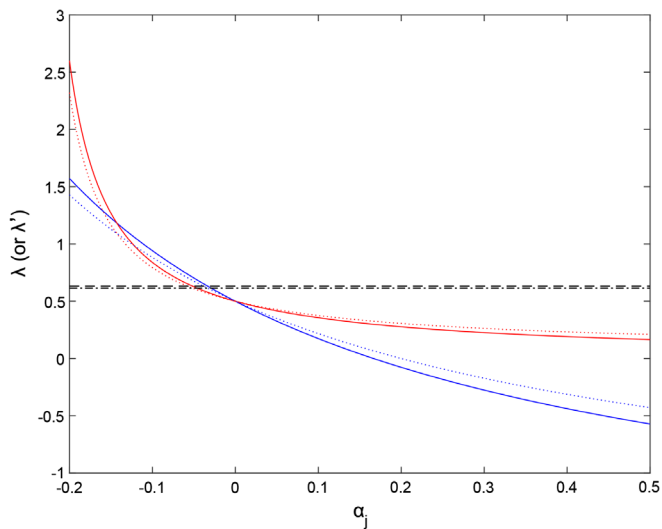


FIG. 3. The behavior of λ_I (or λ'_I) as a function of interacting constant for two simple cases of model I. The black dashed line represents the result of Obs. 1999 for the first possibility, and the dot-dashed line shows this for the second possibility. The blue lines are related to the case of $\alpha_x = 0$, and the red lines indicate model I with $\alpha_c = 0$. Here, the solid lines describe the first possibility, while the dotted lines are attributed to the second possibility.

not display the outcomes of the other four observational datasets to avoid an overcrowded graph.

For both situations of model I, large negative values of α_j are too far away from the observational results. As the interacting constants are declining, both cases reach observational outcomes just before the zero points. Although model I with $\alpha_x = 0$ almost keeps its slope for positive values, the case of $\alpha_c = 0$ remains stable and would be rather comparable with observational results if λ and λ' were less than 0.5, even for higher values of α_x . According to the definition of Q for model I, it means that if the transfer of energy from DE to DM primarily stemmed from the density of DE different values for interacting constant would not lead to considerable changes in the virial condition. In other words, whether the protocluster consists of a dense region of DE or not, there would be merely negligible differences. However, it does not have great practical importance, since we initially assumed that the distribution of DE is unchanged through the interior and exterior of the collapsing sphere. On the contrary, if the energy transfer between DE and DM were mostly affected by the density of DM, the virial theorem would gradually change with interacting constant.

Description of model I in general (without any zero constant) is more elaborate. Nonetheless, several constraints have been yet derived. For example, Ref. [11] obtains four constraints between α_c and α_x . In our study, Eq. (57) gives rise to another constraint for these two parameters:

$$0 < \frac{1 - 6\alpha_c}{2 + 3\alpha_c + 3\alpha_x/R} < \frac{2 - \nu}{2}. \quad (76)$$

Figure 4 illustrates how different inputs of α_c and α_x give different amounts of λ_I , for a small range from -0.1 to 0.1 as an example. Colors denote different values of λ_I for each given α_c and α_x . The red line also constrains acceptable choices for these two parameters, according to Eq. (76). Here, we chose the value of $c = 5$ for a typical cluster and used NFW density profile to calculate ν . All the points in the left-bottom corner of the figure (below the red line) are unacceptable and have no physical meaning due to our recent constraint. In this specific region, which has been deliberately chosen to be close to noninteracting models, every couple with $\alpha_c = -\alpha_x$ gives approximately the same value for λ_I , while $\alpha_c = \alpha_x$ results in very different numbers.

For models II, III, and IV, there is only one interacting constant. For model II, Fig. 5 makes a comparison between observational data and the outcome of obtained values for ξ_1 in Ref. [13]. Similar to the previous cases, the result of $SNeIa + H_0$, which has given $\xi_1 = -0.53$, violates Eq. (57) and leads to negative temperatures. Despite model I, $SNeIa + H_0 + CC$ (with $\xi_1 = -0.07$) results in an allowable prediction for the M-T relation, which is

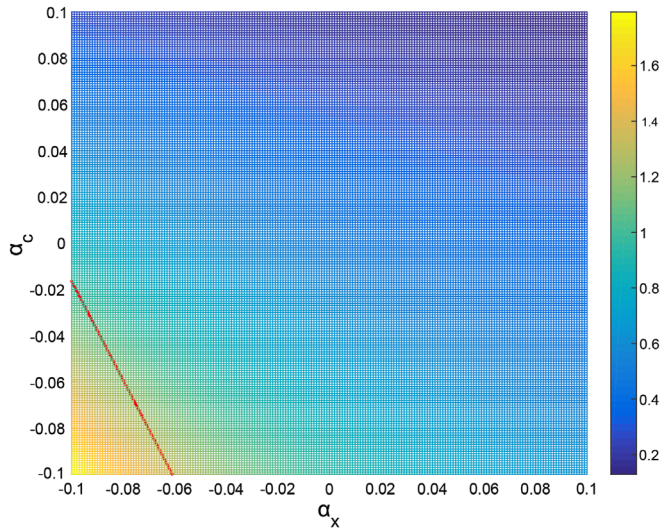


FIG. 4. Different combinations of α_c and α_x in the range between -0.1 to 0.1 result in the value of λ_l from just less than 0.2 to over 1.6 , as is illustrated in this figure. Colors stand for the given value of λ_l for any given couple of α_c and α_x , according to the guide strip in the right side. The red line specifies the obtained constraint, which confines real physical choices.

represented with the purple lines in Fig. 5. The characteristics of the other lines are selected similar to Figs. 1 and 2, with $\xi_1 = -0.06$ for *SNeIa* + H_0 + CC + BAO and $\xi_1 = -0.010$ for *PlanckTT*. In this model, predictions of *SNeIa* + H_0 + CC and *SNeIa* + H_0 + CC + BAO are close to some observational data. For example, the *SNeIa* + H_0 + CC + BAO result of the second possibility in the NFW density profile and also the outcome of *SNeIa* + H_0 + CC for the first possibility in the Burkert

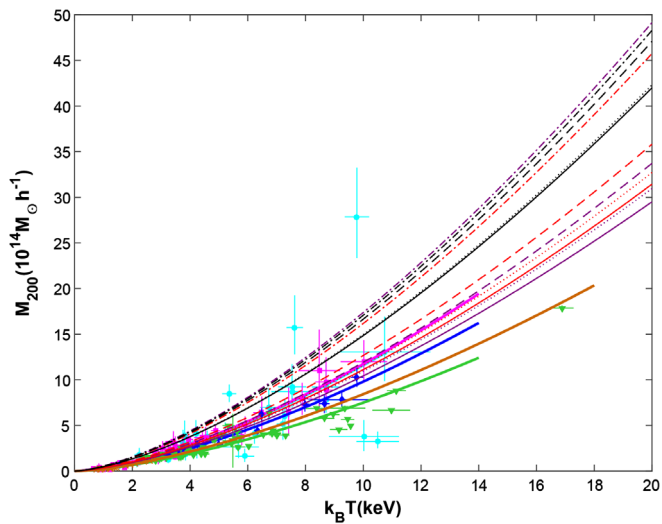


FIG. 5. The M-T diagram of galaxy clusters based on model II. The features are identical to Figs. 1 and 2, except for the purple lines, which have emerged because the predicted value from *SNeIa* + H_0 + CC observations is allowable in this model.

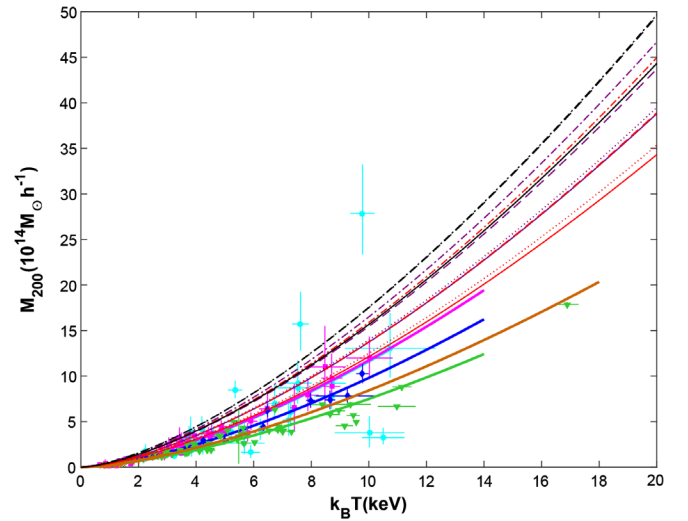


FIG. 6. The M-T diagram for model III; all chosen colors and types of lines are analogous to Fig. 5.

density profile are approximately in agreement with Obs. 1999 and Obs. 2001.

Similarly, Fig. 6 shows the M-T relation for three allowable values of ξ_2 in model III and compares them with fitted curves of the five observational datasets. Here, the values have been proposed as $\xi_2 = -0.40$ for *SNeIa* + H_0 (unacceptable), $\xi_2 = -0.04$ for *SNeIa* + H_0 + CC (purple lines), $\xi_2 = -0.08$ for *SNeIa* + H_0 + CC + BAO (red lines), and $\xi_2 = -0.0024$ for *PlanckTT* (black lines). It is clear that merely the results of *SNeIa* + H_0 + CC + BAO for the NFW density profile are almost close to Obs. 1999 and Obs. 2001, and, again, the other predictions show higher masses than datasets.

For model IV, it is not possible for the result of *SNeIa* + H_0 + CC ($\xi_3 = -0.27$) to indicate an actual illustration of the M-T relation, while the outcomes of *SNeIa* + H_0 ($\xi_3 = -0.23$), although just for NFW profile, in addition to the results of *SNeIa* + H_0 + CC + BAO ($\xi_3 = -0.038$) and *PlanckTT* ($\xi_3 = -1.36 \times 10^{-6}$) are credible. Figure 7 represents these three predictions and compares them with observational datasets. In this graph, the prediction of *SNeIa* + H_0 is displayed by yellow lines, and its first possibility of the NFW density profile is virtually consistent with Obs. 2015.

The evolution of λ as a function of ξ_i (with $i = \text{II, III, IV}$) for models II, III, and IV are presented in Fig. 8. The brown, green, and magenta lines are related to models II, III, and IV, respectively. Like in Fig. 3, black lines describe the obtained value from Obs. 1999 in which the solid lines are drawn for the first possibility and dotted lines show the second possibility. It demonstrates that, while the λ gradually decreases with the growth of ξ_i in models III and IV, it sharply falls for model II.

Model V is the most complicated one. In addition to the fact that there are two interacting parameters, there is also

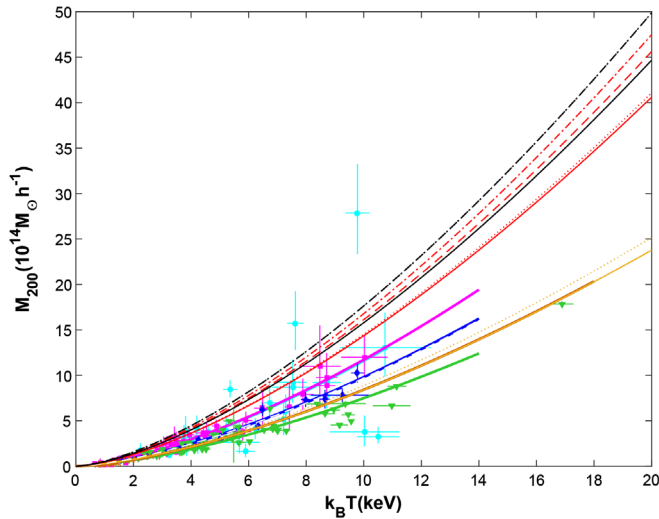


FIG. 7. The behavior of the M-T relation for the predicted values of model IV. Yellow lines represent the observations of $SNeIa + H_0$, and the other colors and types of lines are chosen completely the same as the previous M-T graphs.

an important dependency on H (and therefore redshift z), which means that λ evolves with time. Although Ref. [13] does not investigate model V, Ref. [11] claims that Γ_x and Γ_c should have opposite signs. As a second condition, it is possible to use Eq. (57) to constrain interacting constants. Figure 9 shows the evolution of λ with time, for the simple cases of $\Gamma_x = 0$ or $\Gamma_c = 0$. The horizontal axis indicates $\frac{H(z)}{H_0}$ from the present time to approximately $z = 0.75$, when

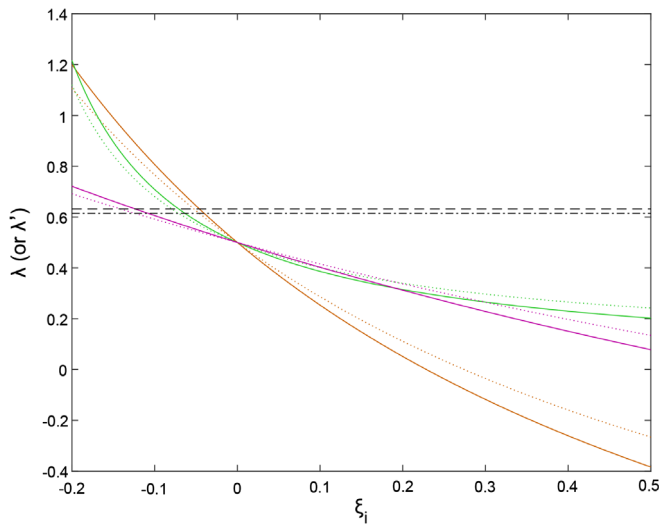


FIG. 8. The changes of λ or λ' as a function of interacting constant in models II, III, and IV. The black dashed line and black dot-dashed line display the first and second possibilities for Obs. 1999, respectively. The behavior of the three mentioned models are shown with brown (model II), green (model III), and magenta (model IV) lines.

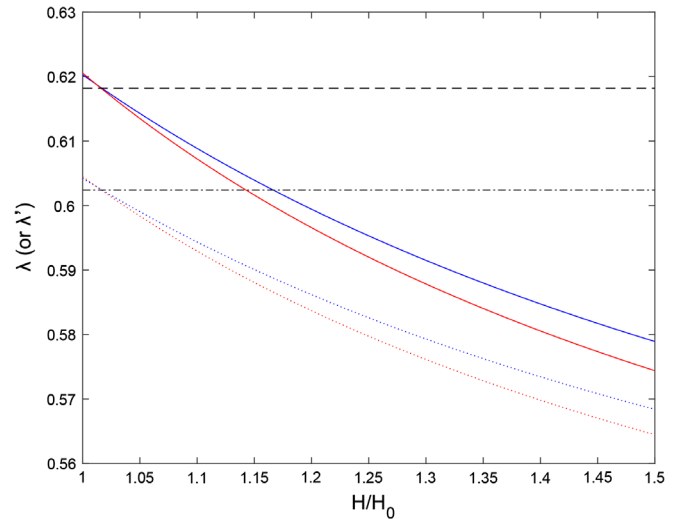


FIG. 9. The figure demonstrates how λ and λ' evolve with time, considering model V. Red and blue lines are related to $\Gamma_x = 0$ and $\Gamma_c = 0$, respectively, and black lines denote the result of Obs. 2001 (with dashed line and solid lines representing the first possibility and the dot-dashed line and dotted lines standing for the second possibility).

$\frac{H(z)}{H_0} = 1.5$. The blue lines are related to the case of $\Gamma_x = 0$, and the red lines describe the case of $\Gamma_c = 0$. Solid lines and dotted lines denote the first and the second possibilities, respectively. As an observational example, we used the result from Obs. 2001, regarding the first (black dashed line) and the second (black dot-dashed line) possibilities. According to this graph, the farther away the cluster is located, the more noticeable difference between the cases of $\Gamma_x = 0$ and $\Gamma_c = 0$ can be seen. All the lines are consistent with observational data in a low redshift, since we fixed the value of interacting constants with regard to this observational dataset itself, so it is not an interesting point. In addition, the figure clearly reveals that the constant of the virial condition was much lower than its present value in the past. It means that further clusters in interacting model V must behave more similarly to the noninteracting model.

The core of our work is to determine interacting constants with respect to observational datasets for mass and temperature of galaxy clusters. As has been mentioned before, we tried to find λ_i (and λ'_i) in a way that the M-T relation could accurately fit the observational curves. Tables I and II summarize the information which has been obtained for all situations, including NFW and Burkert density profiles, the first and the second possibilities, five observational datasets, and seven preferred and discussed cases of models I to V. As far as the constants are concerned, we obtained negative values for all of them. Our results are in agreement with Ref. [13] in terms of obtaining negative values for these constants. It means that energy transfer occurs from DM to DE.

TABLE I. The calculated constants of interacting models regarding the first possibility, based on making comparison with observational datasets of mass and temperature in galaxy clusters.

		$\alpha_c (\alpha_x = 0)$	$\alpha_x (\alpha_c = 0)$	ξ_1	ξ_2	ξ_3	$\gamma_c (\gamma_x = 0)$	$\gamma_x (\gamma_c = 0)$
NFW	Obs. 1999	-0.0334	-0.0517	-0.0459	-0.0709	-0.1235
	Obs. 2001	-0.0301	-0.0472	-0.0412	-0.0647	-0.1110	-0.0306	-0.0481
	Obs. 2006	-0.0547	-0.0764	-0.0750	-0.1048	-0.2019	-0.0577	-0.0806
	Obs. 2009	-0.0891	-0.1078	-0.1222	-0.1478	-0.3290	-0.0919	-0.1111
	Obs. 2015	-0.0653	-0.0871	-0.0896	-0.1195	-0.2412	-0.0660	-0.0881
Burkert	Obs. 1999	-0.0519	-0.0734	-0.0711	-0.1007	-0.1915
	Obs. 2001	-0.0488	-0.0701	-0.0670	-0.0961	-0.1803	-0.0497	-0.0713
	Obs. 2006	-0.0747	-0.0958	-0.1024	-0.1314	-0.2758	-0.0788	-0.1010
	Obs. 2009	-0.1117	-0.1242	-0.1532	-0.1703	-0.4125	-0.1152	-0.1280
	Obs. 2015	-0.0880	-0.1070	-0.1207	-0.1467	-0.3251	-0.0890	-0.1081

TABLE II. The calculated constants of interacting models regarding the second possibility, based on making comparison with observational datasets of mass and temperature in galaxy clusters.

		$\alpha_c (\alpha_x = 0)$	$\alpha_x (\alpha_c = 0)$	ξ_1	ξ_2	ξ_3	$\gamma_c (\gamma_x = 0)$	$\gamma_x (\gamma_c = 0)$
NFW	Obs. 1999	-0.0292	-0.0461	-0.0400	-0.0632	-0.1077
	Obs. 2001	-0.0262	-0.0420	-0.0360	-0.0576	-0.0968	-0.0267	-0.0427
	Obs. 2006	-0.0479	-0.0691	-0.0657	-0.0947	-0.1769	-0.0506	-0.0729
	Obs. 2009	-0.0786	-0.0992	-0.1078	-0.1360	-0.2903	-0.0811	-0.1023
	Obs. 2015	-0.0574	-0.0792	-0.0787	-0.1086	-0.2118	-0.0580	-0.0801
Burkert	Obs. 1999	-0.0454	-0.0663	-0.0623	-0.0909	-0.1677
	Obs. 2001	-0.0427	-0.0631	-0.0586	-0.0866	-0.1578	-0.0435	-0.0642
	Obs. 2006	-0.0657	-0.0875	-0.0901	-0.1200	-0.2427	-0.0693	-0.0923
	Obs. 2009	-0.0990	-0.1154	-0.1358	-0.1582	-0.3657	-0.1021	-0.1189
	Obs. 2015	-0.0777	-0.0984	-0.1065	-0.1349	-0.2868	-0.0785	-0.0995

In model V, it is common to define the dimensionless constants $\gamma_j = \frac{\Gamma_j}{H_0}$ and write λ_V as

$$\lambda_V = \frac{\frac{H(z)}{H_0} - 6\gamma_c}{2\frac{H(z)}{H_0} + 3\gamma_c + 3\gamma_x/R}. \quad (77)$$

Therefore, we calculated the constants γ_j rather than Γ_j .

From the calculated constants, it can be concluded that more negative values are needed for a cored density profile (Burkert) than a cuspy profile (NFW) to be consistent with each observational dataset.

Note that even fine differences among observational results may play considerable roles in the calculated constants. In fact, in our method, every input value in Eq. (46) contributes to measuring interacting constants. However, we strove to incorporate as many various assumptions as possible (embracing different density profiles, different possibilities, and different observational datasets) in order to compensate for the inaccuracies of parameters within Q .

V. CONCLUSION

We investigated the mass-temperature relation of galaxy clusters for a number of interacting models of dark matter

and dark energy, which are summarized in Eq. (7). First of all, we expanded the method provided in Ref. [25] to derive the modified virial theorem for all these models of the interacting dark sector in Sec. II. It immediately suggested that there might be two different possibilities for this condition, regarding two plausible behaviors of dark matter through baryonic matter. Then, we used the modified virial condition to obtain the M-T relation with respect to three different procedures in Sec. III. It revealed that the effect of interaction only emerges within the normalization factor of the M-T relation.

The M-T relation led to a new constraint on interacting constants, which totally depends on the concentration parameter and density profile of the clusters [Eq. (57)]. This constraint is used to check the suggested constants of interacting and showed that many of those suggested values are not acceptable, due to resulting in negative masses for given temperatures.

To analyze the obtained M-T relation, we focused on five different observational datasets and compared their fitted lines with many suggested values for interacting constants. We considered two outstanding density profiles, which are NFW and Burkert, and managed to calculate interacting constants for seven cases of the five interacting models. Overall, it appears that according to these observational

datasets energy transfer should occur from DM to DE, which leads to negative values for interacting constants. It is completely consistent with the results of Ref. [13], which has investigated many other observational constraints to obtain numerical values for interacting constants. Although different observations result in minuscule differences in the figures, the figures are usually near zero. Furthermore, the positive constants can solely be obtained for models I and V, if both constants have nonzero values. It also appears that for a cored density profile more negative constants are obtained in comparison with a cuspy profile.

While the M-T relation and interacting constants were being studied, we also allocated some parts of this paper to discuss how the ratio of kinetic to the potential energy of a virialized cluster behaves as a function of interacting constants or redshift, for many of our interacting models. Figures 3 and 8 show that various models of interaction cause different behaviors of λ as a function of interacting constant, although all of them lead to decreasing functions. The graphs also indicated that for model V the value of λ grows with time, resulting in the fact that more distant clusters must be theoretically more consistent with non-interacting models. Two specific cases of this model ($\Gamma_x = 0$ and $\Gamma_c = 0$) are also more distinguishable from each other when the cluster is located in a higher redshift.

Finally, we emphasized that the obtained values could be extremely affected by the other parameters in the normalization factor of the M-T relation, which we have fixed with particular values for our research. However, considering a variety of possibilities might have compensated for these unwanted errors and impacts to some extent.

We should also mention that future observations of cluster masses and temperatures may assist in obtaining more exact numerical values for interacting constants. To this purpose, cluster masses should be determined via the other methods of mass measurement, such as gravitational lensing, instead of obtaining the mass from x-ray temperature. The Euclid satellite and large synoptic survey telescope (LSST) are two upcoming projects which would provide improved mass data through gravitational lensing observations. To have a better temperature dataset, eROSITA is one of the x-ray surveys that would help. In addition, future simulations with regard to verified assumptions according to observational results can suggest improved density profile and velocity dispersion for galaxy clusters and consequently play a beneficial role in the certainty of our calculations. The impact of velocity dispersion emerges in $\tilde{\beta}_{\text{spec}}$. Clearly, any change in the assumed characteristics of the halo profile can affect the final outcomes.

-
- [1] G. Bertone, D. Hooper, and J. Silk, *Phys. Rep.* **405**, 279 (2005).
- [2] E. S. Battistelli *et al.*, *Int. J. Mod. Phys. D* **25**, 1630023 (2016).
- [3] A. Challinor, *IAU Symp.* **8**, 42 (2013).
- [4] M. Kilbinger, *Rep. Prog. Phys.* **78**, 086901 (2015).
- [5] A. Del Popolo, *Astronomy Reports* **51**, 169 (2007).
- [6] J. Einasto, *ASP Conf. Ser.* **252**, 85 (2001).
- [7] M. Klasen, M. Pohl, and G. Sigl, *Prog. Part. Nucl. Phys.* **85**, 1 (2015).
- [8] A. G. Riess *et al.* (Supernova Search Team), *Astron. J.* **116**, 1009 (1998).
- [9] A. V. Astashenok and A. del Popolo, *Classical Quantum Gravity* **29**, 085014 (2012); H. E. S. Velten, R. F. vom Martens, and W. Zimdahl, *Eur. Phys. J. C* **74**, 3160 (2014); S. Weinberg, *Rev. Mod. Phys.* **61**, 1 (1989).
- [10] G. R. Farrar and P. J. E. Peebles, *Astrophys. J.* **604**, 1 (2004).
- [11] G. Caldera-Cabral, R. Maartens, and L. A. Urena-Lopez, *Phys. Rev. D* **79**, 063518 (2009).
- [12] A. A. Costa, X. D. Xu, B. Wang, and E. Abdalla, *J. Cosmol. Astropart. Phys.* **01** (2017) 028; W. Yang, S. Pan, E. Di Valentino, R. C. Nunes, S. Vagnozzi, and D. F. Mota, *J. Cosmol. Astropart. Phys.* **09** (2018) 019; E. Di Valentino, A. Melchiorri, O. Mena, and S. Vagnozzi, *Phys. Dark Universe* **30**, 100666 (2020).
- [13] R. von Martens, L. Casarini, D. F. Mota, and W. Zimdahl, *Phys. Dark Universe* **23**, 100248 (2019).
- [14] C. Llinares, A. Knebe, and H. Zhao, *Mon. Not. R. Astron. Soc.* **391**, 1778 (2008); G. B. Zhao, B. Li, and K. Koyama, *Phys. Rev. D* **83**, 044007 (2011); E. Puchwein, M. Baldi, and V. Springel, *Mon. Not. R. Astron. Soc.* **436**, 348 (2013); C. Llinares, D. F. Mota, and H. A. Winther, *Astron. Astrophys.* **562**, A78 (2014); M. B. Gronke, C. Llinares, and D. F. Mota, *Astron. Astrophys.* **562**, A9 (2014).
- [15] S. Bhattacharya, K. F. Dialektopoulos, A. E. Romano, C. Skordis, and T. N. Tomaras, *J. Cosmol. Astropart. Phys.* **07** (2017) 018; R. C. C. Lopes, R. Voivodic, L. R. Abramo, and L. Sodir, Jr., *J. Cosmol. Astropart. Phys.* **09** (2018) 010.
- [16] S. Adhikari, J. Sakstein, B. Jain, N. Dalal, and B. Li, *J. Cosmol. Astropart. Phys.* **11** (2018) 033.
- [17] A. Hammami and D. F. Mota, *Astron. Astrophys.* **598**, A132 (2017).
- [18] N. Afshordi and R. Cen, *Astrophys. J.* **564**, 669 (2002).
- [19] A. D. Popolo, *Mon. Not. R. Astron. Soc.* **336**, 81 (2002).
- [20] A. Del Popolo, F. Pace, and D. F. Mota, *Phys. Rev. D* **100**, 024013 (2019).
- [21] G. Caldera-Cabral, R. Maartens, and B. M. Schaefer, *J. Cosmol. Astropart. Phys.* **07** (2009) 027.
- [22] R. Javadinzhad, J. T. Firouzjaee, and R. Mansouri, *Phys. Rev. D* **93**, 023007 (2016).

- [23] T. Harko and K. S. Cheng, *Phys. Rev. D* **76**, 044013 (2007); N. S. Santos and J. Santos, *J. Cosmol. Astropart. Phys.* **12** (2015) 002.
- [24] J. H. He, B. Wang, E. Abdalla, and D. Pavon, *J. Cosmol. Astropart. Phys.* **12** (2010) 022.
- [25] J. H. He, B. Wang, and Y. P. Jing, *J. Cosmol. Astropart. Phys.* **07** (2009) 030.
- [26] D. Layzer, *Astrophys. J.* **138**, 174 (1963).
- [27] P. A. R. Ade *et al.* (Planck Collaboration), *Astron. Astrophys.* **594**, A24 (2016).
- [28] R. C. Batista and V. Marra, *J. Cosmol. Astropart. Phys.* **11** (2017) 048.
- [29] C. C. Chang, W. Lee, and K. W. Ng, *Phys. Dark Universe* **19**, 12 (2018).
- [30] O. Muanwong, P. A. Thomas, S. T. Kay, F. R. Pearce, and H. M. P. Couchman, *Astrophys. J. Lett.* **552**, L27 (2001).
- [31] J. J. Bialek, A. E. Evrard, and J. J. Mohr, *Astrophys. J.* **555**, 597 (2001).
- [32] R. Stanek, E. Rasia, A. E. Evrard, F. Pearce, and L. Gazzola, *Astrophys. J.* **715**, 1508 (2010).
- [33] S. Planelles, S. Borgani, D. Fabjan, M. Killedar, G. Murante, G. L. Granato, C. Ragone-Figueroa, and K. Dolag, *Mon. Not. R. Astron. Soc.* **438**, 195 (2014).
- [34] E. L. Lokas and G. A. Mamon, *Mon. Not. R. Astron. Soc.* **321**, 155 (2001).
- [35] A. Burkert, *IAU Symp.* **171**, 175 (1996); *Astrophys. J. Lett.* **447**, L25 (1995).
- [36] A. V. Maccio', A. A. Dutton, and F. C. v. d. Bosch, *Mon. Not. R. Astron. Soc.* **391**, 1940 (2008).
- [37] S. Bhattacharya, S. Habib, K. Heitmann, and A. Vikhlinin, *Astrophys. J.* **766**, 32 (2013).
- [38] B. S. Ryden, *Astrophys. J.* **329**, 589 (1988).
- [39] A. D. Popolo and M. Gambera, *Astron. Astrophys.* **337**, 96 (1998).
- [40] O. Lahav, P. B. Lilje, J. R. Primack, and M. J. Rees, *Mon. Not. R. Astron. Soc.* **251**, 128 (1991).
- [41] S. Colafrancesco, V. Antonuccio-Delogu, and A. D. Popolo, *Astrophys. J.* **455**, 32 (1995).
- [42] G. M. Voit, *Astrophys. J.* **543**, 113 (2000).
- [43] D. J. Horner, R. F. Mushotzky, and C. A. Scharf, *Astrophys. J.* **520**, 78 (1999).
- [44] A. Finoguenov, T. H. Reiprich, and H. Boehringer, *Astron. Astrophys.* **368**, 749 (2001).
- [45] A. Vikhlinin, A. Kravtsov, W. Forman, C. Jones, M. Markevitch, S. S. Murray, and L. Van Speybroeck, *Astrophys. J.* **640**, 691 (2006).
- [46] A. Vikhlinin, R. A. Burenin, H. Ebeling, W. R. Forman, A. Hornstrup, C. Jones, A. V. Kravtsov, S. S. Murray, D. Nagai, H. Quintana, and A. Voevodkin, *Astrophys. J.* **692**, 1033 (2009).
- [47] L. Lovisari, T. Reiprich, and G. Schellenberger, *Astron. Astrophys.* **573**, A118 (2015).
- [48] B. F. Mathiesen and A. E. Evrard, *Astrophys. J.* **546**, 100 (2001).
- [49] D. J. Horner, R. F. Mushotzky, and C. A. Scharf, *Astrophys. J.* **520**, 78 (1999).